Development 133, 3139-3146 (2006) doi:10.1242/dev.02469

santa and *valentine* pattern concentric growth of cardiac myocardium in the zebrafish

John D. Mably*, Lesley P. Chuang, Fabrizio C. Serluca†, Manzoor-Ali P. K. Mohideen‡, Jau-Nian Chen§ and Mark C. Fishman*,†

During embryogenesis, the myocardial layer of the primitive heart tube grows outward from the endocardial-lined lumen, with new cells added to generate concentric thickness to the wall. This is a key evolutionary step, demarcating vertebrates from more primitive chordates, and is essential for normal cardiac function. Zebrafish embryos with the recessive lethal mutations *santa* (*san*) and *valentine* (*vtn*) do not thicken, but do add the proper number of cells to the myocardium. Consequently, the heart chambers are huge, constituted of a monolayered myocardium lined by endocardium. This phenotype is similar to that of the *heart of glass* (*heg*) mutation, which we described previously as a novel endocardial expressed gene. By positional cloning, we here identify *san* as the zebrafish homolog of human CCM1, and *vtn* as the homolog of human CCM2. Dominant mutations of either in humans cause vascular anomalies in the brain, known as cerebral cavernous malformations. The synergistic effects of morpholino pairs indicate that *san*, *vtn* and *heg* are in a genetic pathway, and *san* and *vtn* contain protein motifs, NPxY and PTB domain, respectively, known to interact. This suggests that concentric growth of the myocardium, crucial for blood pressure generation, is dictated by a *heg-san-vtn* signaling pathway.

KEY WORDS: *santa*, *valentine*, Myocardial growth, Cerebral cavernous malformations, CCM

INTRODUCTION

A central question of developmental biology is how vertebrate organs acquire their form. For the heart, part of such morphogenesis reflects control of overall cell number (Rottbauer et al., 2001; Rottbauer et al., 2002). Others control development of cells along two axes: anterior-posterior (Stainier and Fishman, 1992) and concentric (Mably et al., 2003). During the first stage of primitive heart tube formation the heart grows in essentially an anterior-posterior direction, with each of the two chambers constituted by a single-layered myocardium around the single layer of endocardium. The onset of concentric growth is marked by the addition of new cells in the myocardium in a direction perpendicular to the lumen, an outward growth that thickens the wall in a concentric direction, especially in the ventricle.

We have identified three mutations that block concentric growth without affecting overall cell number or the organization of anterior-posterior growth. We recently cloned one of these, *heart of glass* (*heg*), which turned out to be a novel gene, expressed in the endocardium. Here we focus on the other two genes, *santa* (*san*) and *valentine* (*vtn*). By positional cloning, we identify *san* as the zebrafish homolog of human CCM1 (KRIT1) (Laberge-le Couteulx et al., 1999; Sahoo et al., 1999) and *vtn*, the zebrafish homolog of human CCM2 (Denier et al., 2004). Mutations in these genes in humans have been implicated in the autosomal dominant disease, cerebral cavernous malformations (CCM).

Evidence from potential interacting protein motifs, and from cross-sensitization of phenotype though morpholino injection, suggests that *san*, *vtn* and *heg* may interact. This suggests that concentric growth of the ventricle is an essential element of cardiac patterning, controlled at least in part by signals from the endocardium, and involving a pathway comprised of *san*, *vtn* and *heg*.

Cardiovascular Research Center, Massachusetts General Hospital and the Department of Medicine, Harvard Medical School, 149 13th Street, Charlestown, MA 02129, USA.

*Authors for correspondence (e-mail: jmably@partners.org; mark.fishman@novartis.com)
†Present address: The Novartis Institutes for Biomedical Research, Cambridge, MA 02139, USA
‡Present address: Case Western Reserve University, 11119 Bellflower Road, 150 PBL, Cleveland, OH 44106-7235, USA
§Present address: Department of Molecular, Cell and Developmental Biology, University of California Los Angeles, Life Sciences Building, Rm 5109, 621 Charles E. Young Drive South, Los Angeles, CA 90095, USA

Accepted 1 June 2006

MATERIALS AND METHODS

Histological sectioning and cell counting

Histology was performed on paraformaldehyde-fixed embryos embedded in plastic (JB-4, Polysciences, Inc.). Sectioning was performed using a Jung supercut 2065 at 5 μm setting.

The zebrafish cardiac myosin light chain-2 (*cmlc2*) promoter-DsRed (red fluorescent protein) line has been described previously (Mably et al., 2003). Transgenic *cmlc2:DsRed2-nuc* zebrafish were bred with *san* heterozygotes. The progeny were raised and incrossed to identify *san* heterozygotes expressing red fluorescent protein (RFP). The embryos from these clutches were scored for the *san* phenotype. Wild-type siblings and mutant embryos were raised at 28.5°C until 48 or 72 hours post fertilization (hpf), at which time the embryos were flat-mounted and RFP-positive myocardial cells were counted (Mably et al., 2003; Shu et al., 2003). Morpholino-injected transgenic *cmlc2:DsRed2-nuc* embryos were analyzed in a similar manner. The same flat-mount technique was used to determine endocardial cell number in morpholino-injected transgenic *(fli1:nEGFP)*^{y7} embryos (Roman et al., 2002). The nuclear localization of each fluorescent protein facilitates easier determination of cell number.

Positional cloning

Embryos were separated into mutant and wild-type pools based on phenotypic analysis. Genomic DNA was isolated from individual embryos by incubation in DNA isolation buffer overnight at 50°C (DNA isolation buffer: 10 mmol/l Tris-HCl, pH 8.3; 50 mmol/l KCl; 0.3% Tween-20; 0.3% Nonidet P40; 0.5 mg/ml proteinase K). Proteinase K was inactivated before PCR setup by heating samples to 98°C for 10 minutes. PCR reactions were performed using diluted genomic DNA as described (Knapik et al., 1996).

Bulked segregant analysis (Michelmore et al., 1991) and identification of the critical genetic interval was performed essentially as described previously (Mably et al., 2003). To identify the *san* gene, bacterial artificial chromosome (BAC) clones 92i12 and 184d07 (see Fig. S3 in the supplementary material) were sequenced by shotgun cloning of partial *Alu*I and *Sau*3AI digested fragments subcloned into pBluescript. Sequence analysis was performed on an ABI3700 to generate approximately fivefold coverage. The sequence was assembled using the Phred/Phrap/Consed programs (Ewing and Green, 1998; Ewing et al., 1998; Gordon et al., 1998). The *vtn* gene was identified through morpholino analysis of genes identified as candidates by position through synteny with the *Takifugu rubripes* (fugu) genome, followed by sequencing of cDNA and genomic DNA from mutant and wild-type embryos.

RNA isolation and real-time PCR analysis

RNA was isolated using trizol (Invitrogen) or RNeasy columns (Qiagen) as instructed by the manufacturer. For determination of the mRNA transcript variants induced by the splice site blocking morpholinos, the QIAGEN OneStep RT-PCR (reverse transcriptase polymerase chain reaction) kit was used with primers designed from exons on either side of the morpholino target. The PCR primers used to detect the splice variants induced by the various morpholinos are summarized as follows.

san exon 1 donor: san_exon01_F1, 5′-AAAGAGGAGCTGCATGATGG-3′; san_exon02_R1, 5′-ATATGGGCTTGGTGGTTTCA-3′

san exon 14 donor: san_exon12_F1, 5′-TAGCCTCCTCCTGCAGATCA-3′; san_exon16_R1, 5′-CTTCATCAGCAGCTTCACGA-3′

vtn exon 2 donor: vtn_exon01_F1, 5′-TGAAGAGCATTTGTACGTAGAG-3′; vtn_exon04_R1, 5′-TCTCTGATGTAGGACACAGC-3′

Analysis of mRNA levels in the *san* wild type and –/– (mutant) embryos was performed using the Qiagen QuantiTect® SYBR® Green RT-PCR kit, as described by the manufacturer (Qiagen). The primers used for this analysis were designed to exon 13 (5′-GAGCAAAGCACATCACTGGA-3′) and exon 14 (5′-ATCACCTTGTGTGTGCTGGA-3′).

DNA cloning and RNA rescue

For RT-PCR analysis, RNA was isolated (RNeasy columns, Qiagen) from pools of wild-type and mutant embryos. cDNA was amplified using RACE (SMART RACE cDNA amplification kit, Clontech). Fragments were then subcloned into PCRII-TOPO (Invitrogen). The 5′ end of the *san* cDNA was amplified by 5′ RACE with a primer designed from the full-length cDNA predicted by Genscan (Burge and Karlin, 1998) (5′-TTCAGCAGGTTGGGGGTTACAGTTGC-3′). A 3′ RACE product was generated using a primer (5′-TCTCAGTCAAACAGCTGGACAGCGAC-3′) designed to amplify an overlying fragment of the *san* cDNA. Both cDNA fragments were digested with *Sph*I (a unique restriction site within the overlapping region) and *Eco*RI then ligated into *Eco*RI-digested pCS2 vector (Turner and Weintraub, 1994) to create the full-length *san* cDNA construct. Clones with the correct orientation were identified by sequencing (GenBank Accession Number DQ677877).

The full-length *vtn* cDNA was amplified using primers designed to the 5′ and 3′UTR sequences within the Genscan predicted cDNA (5′UTR_F1, AATACAGCGAAAATGAAGAGCA; 3′UTR_R1, CAGCATCCAAACTTTCAGCA). The PCR product was subcloned into pCRII-TOPO (Invitrogen). The *vtn* cDNA was excised from pCRII-TOPO by digestion with *Eco*RI, and then subcloned into *Eco*RI-digested pCS2 (Turner and Weintraub, 1994). Clones with the correct orientation were identified by sequencing (GenBank Accession Number DQ677878).

Injection RNA was generated from the full-length pCS2 *san* and *vtn* constructs using the Ambion mMESSAGE mMACHINE kit (digested with *Not*I followed by transcription with SP6 polymerase).

Whole-mount in-situ hybridization and antibody staining

For whole-mount in-situ hybridization and immunohistochemistry, embryos were fixed in 4% paraformaldehyde in phosphate-buffered saline, and then stored in 100% methanol at –20°C. Digoxigenin-labeled antisense RNA probes were generated by in-vitro transcription (Roche), and in-situ hybridization was carried out as previously described (Jowett and Lettice, 1994; Mably et al., 2003). The *san* probe used was derived from a partial EST in pSPORT1, fb36f07 (GenBank accession: AI415912, digested with *Eco*RI followed by transcription with SP6 polymerase). The *vtn* probe was derived from the full-length pCS2 construct described previously (digested with *Bam*HI followed by transcription with T7 polymerase). Embryos were allowed to develop in BM purple (Roche) at 28°C, then stopped by several rinses in 1XPBT and stored at 4°C.

Antibody staining with the S46 and MF20 antibodies (Developmental Studies Hybridoma Bank, University of Iowa) was performed as previously described (Mably et al., 2003; Yelon et al., 1999).

Morpholino analysis

The antisense morpholino oligonucleotide designed over the *san* exon 1 donor site [5′-GCTTTATTTCACCTCAC(intron-exon)CTCATAGG-3′, GeneTools, LLC] was dissolved at a concentration of 200 μmol/l in 1× Danieau's buffer [5 mmol/l Hepes pH 7.6, 58 mmol/l NaCl, 0.7 mmol/l KCl, 0.6 mmol/l $Ca(NO3)_2$, 0.4 mmol/l $MgSO_4$]. One nanoliter of this solution or 1× Danieau's buffer was injected into each 1-4 cell embryo before allowing the embryos to develop at 28.5°C. The analysis with the *san* exon 14 donor site morpholino [5′-TTGAAGTCTCAC (intron-exon)TTTTGTCTCCATG-3′, GeneTools, LLC] and *vtn* exon 2 donor site morpholino [5′-GAAGCTGAGTAATAC(intron-exon)CTTAACTTCC-3′, GeneTools, LLC] were performed in the same manner.

RESULTS

santa and *valentine* exhibit defects of the myocardium and cardiac cushions

Both *santa* and *valentine* were identified from a large-scale zebrafish genetic screen, as N-ethyl-N-nitrosourea (ENU)-induced recessive embryonic lethal mutations with massively dilated hearts (Chen et al., 1996; Driever et al., 1996; Stainier et al., 1996). These mutants are unable to generate blood circulation, despite the presence of cardiac contractions. They are distinguishable from their wild-type siblings by 28-30 hpf on this basis, and later by the onset of chamber dilation. The cardiac chambers are dramatically enlarged by 48 hpf.

By contrast to the wild type, in which the myocardial wall is 2-3 cells thick (Fig. 1A), *san* and *vtn* both had only a single layer, in both chambers of the heart (Fig. 1C,E). Cells within the myocardium of both chambers of the heart were differentiated as cardiac cells, indicated by labeling with molecular markers for the atrium (S46 antibody) and ventricle (*ventricular myosin heavy chain*, *vMHC*; Fig. 1B,D,F) (Yelon et al., 1999). Both the endocardial and myocardial layers of the heart were present and individual myocardial cells were thinner than wild type (Fig. 1C′,E′).

By 48 hpf, wild-type zebrafish embryos develop valvular precursors, endocardial cushions, at the atrioventricular junction (Hu et al., 2000). Endocardial cushions were absent in *san* and *vtn* mutant embryos, as determined by neuregulin staining (Milan et al., 2006), and the myocardial and endocardial layers, which were very thin, were closely juxtaposed (Fig. 1; see Fig. S1 in the supplementary material). Electron microscopic (EM) analysis of the structure of cardiomyocytes within the ventricles of *san* and *vtn* hearts revealed the presence of sarcomeres, consistent with the ability of the hearts to contract (see Fig. S2 in the supplementary material). The absence of endocardial cushions and the variations in cellular morphology detected by EM could both be secondary effects of the severe cardiac dilation.

Myocardial and endocardial cell number is normal

The massive enlargement of the *san* and *vtn* hearts could be suggestive of an increase in cell number. To determine cell number, we specifically labeled cardiomyocytes in vivo, using transgenic zebrafish with a red fluorescent protein (DsRed2-nuc) expressed under the control of the *cardiac myosin light chain-2* (*cmlc2*) promoter (Mably et al., 2003; Rottbauer et al., 2002). This assay indicated that the number of myocardial cells was indistinguishable

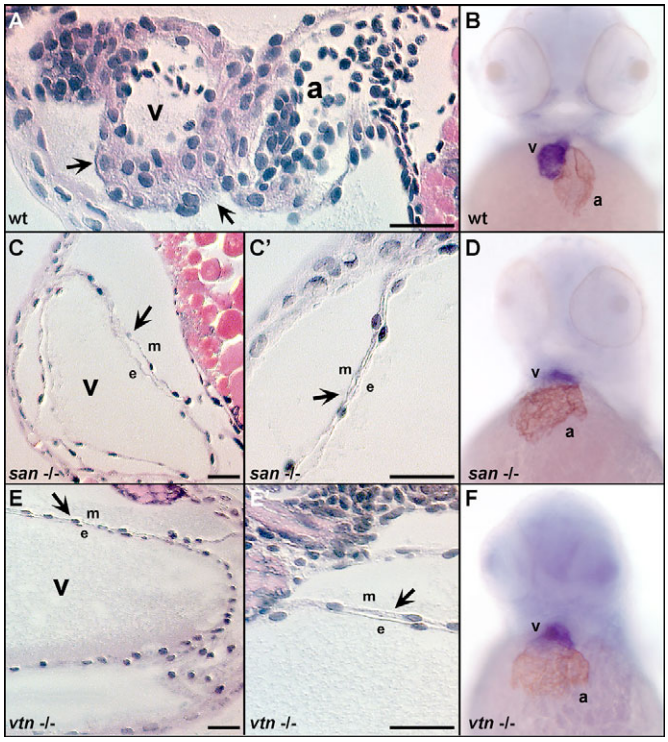

Fig. 1. Morphological analysis of cardiac chambers of *san* and *vtn* mutant embryos. Hematoxylin- and eosin-stained sagittal sections through 72 hpf hearts were used to assess cardiac histology (**A,C,E**). Double-staining using an atrial-specific antibody (S46) and an in-situ RNA probe to the *ventricular myosin heavy chain* (*vMHC*) were used to distinguish the atrial and ventricular chambers (**B,D,F**). The myocardial wall (indicated by arrows) in wild-type hearts (A) is several cell layers thick. However, the myocardium in both *san* (C′) and *vtn* (E′) mutant hearts does not thicken and remains a single cell layer. Both mutants are shown at a reduced magnification in C and E to illustrate the dramatic dilation of the cardiac chambers. The hearts of (B) wild-type, (D) *san*$^{-/-}$, and (F) *vtn*$^{-/-}$ embryos at 48 hpf express markers specific for the two cardiac chambers although the hearts of both mutants are enlarged. Scale bars: 25 μm. a, atrium; e, endocardium; m, myocardium; v, ventricle.

Table 1. The number of cells in *san* mutant hearts and *vtn* morphants is similar to wild type at day 2 of development.

	n	Myocardial cell number ± s.e.m.
Wild-type siblings	4	296±26
san$^{-/-}$	4	295±21
Mock injected	5	273±18
vtn mo	6	273±10
		Endocardial cell number ± s.e.m.
Mock injected	4	151±22
san mo	4	149±8
vtn mo	4	138±8

The myocardial cell counts were determined from flatmounts of progeny generated from *san/cmlc2:DsRed2-nuc* transgenic heterozygotes and from *cmlc2:DsRed2-nuc* transgenic wild types that were either mock injected or injected with the *vtn* exon 2 donor morpholino. The number of myocardial cells was based on the number of RFP-expressing cells present in the hearts of individual animals. (The slight difference between the *san* and *vtn* groups reflect variation in the time during day 2 of development when the counts were made.) The endocardial cell counts were determined from flatmounts of progeny generated from *(fli1:nEGFP)*^{y7} crossed with transgenic *cmlc2:DsRed2-nuc* that were mock injected or injected with the *san* exon 1 donor or *vtn* exon 2 donor morpholinos. The number of endocardial cells was based on the number of GFP-expressing cells present within the heart domain outlined by expression of the RFP transgene.
n, number of hearts counted; wild-type sibs, *san* wild-type siblings; *san*$^{-/-}$, *san* mutants; *vtn* mo, *vtn* exon 2 donor morpholino injected (200 μM); *san* mo, *san* exon 1 donor morpholino injected (200 μM).

between wild-type and *san* mutant embryos and between mock-injected and *vtn* morphant embryos at 2 days post fertilization (dpf) (Table 1). Similarly, we determined the number of endocardial cells in mock-injected and *san* and *vtn* morphant embryos at 2 dpf (Table 1). Morpholinos were injected into the progeny of transgenic *(fli1:nEGFP)*^{y7} crossed with transgenic *cmlc2:DsRed2-nuc* zebrafish. The number of eGFP-expressing cells in the hearts of progeny expressing both the myocardial RFP and endothelial/endocardial eGFP were determined. As noted for the myocardial cell counts, endocardial cell number did not vary from that determined for wild type. Hence, the dilated heart is not caused by an increase in the number of cardiac cells but rather in the manner they are assembled. The myocardial cells stretch in a single layer along the circumference of the cardiac chambers, rather than intercalating to form a thick myocardial wall, resulting in the observed chamber dilation.

Characterization of the *san* and *vtn* genes

san

We positionally cloned both *san* and *vtn* (see Fig. S3 in the supplementary material). The complete *san* gene is comprised of 16 coding exons with a deduced amino acid sequence of 741 amino acids. The human homolog is krit1 (CCM1) (Fig. 2A). The protein is characterized by the presence of several protein domains, including two NPxY motifs (residues 191-194 and 229-232), three ankyrin repeats (residues 285-317, 318-351 and 352-385), and a C-terminal B41/FERM domain (residues 414-638).

The *N*-terminal NPxY motif is conserved in vertebrate species examined and also in the *Caenorhabditis elegans* ortholog (ZK265.1). This motif has been shown to interact with the phosphotyrosine (PTB)-containing protein ICAP1α (Zawistowski et al., 2002; Zhang et al., 2001). In *C. elegans* this sequence is NPXF (Fig. 2A), similar to the elements within the intracellular domain of β2-integrins (Calderwood et al., 2003). The Y→F substitution results in a motif that can still interact with a PTB domain but is not subject to regulation by phosphorylation state (Calderwood et al., 2003). The three ankyrin repeats, believed to be sites of protein-protein interactions (reviewed by Mosavi et al., 2004), and the FERM domain (reviewed by Bretscher et al., 2002), implicated in the association of proteins with the cell membrane, are conserved across species, although the sequence of the FERM domain in the *C. elegans* homolog is poorly conserved and truncated (Fig. 2A).

Sequencing of the m775 (Stainier et al., 1996) *san* cDNA predicts a splicing defect with a consequent in-frame deletion of exon 14. This results from a splice acceptor mutation within the intron at the start of exon 14 (agAG→aaAG; Fig. 2A). The affect on the level of full-length *san* message was confirmed by real-time PCR amplification of m775 mRNA, showing significantly decreased levels of RNA transcripts containing exon 14 (Fig. 2B). In addition we sequenced another *san* allele, ty219c (Chen et al., 1996). This mutation is a C to A transversion within codon 694 of exon 15 (TAC→TAA) that predicts a tyrosine change to a stop codon (Y→stop; Fig. 2A). Both mutations would be predicted to cause loss of a *C*-terminal portion of the Santa protein, possibly disrupting function of the FERM domain.

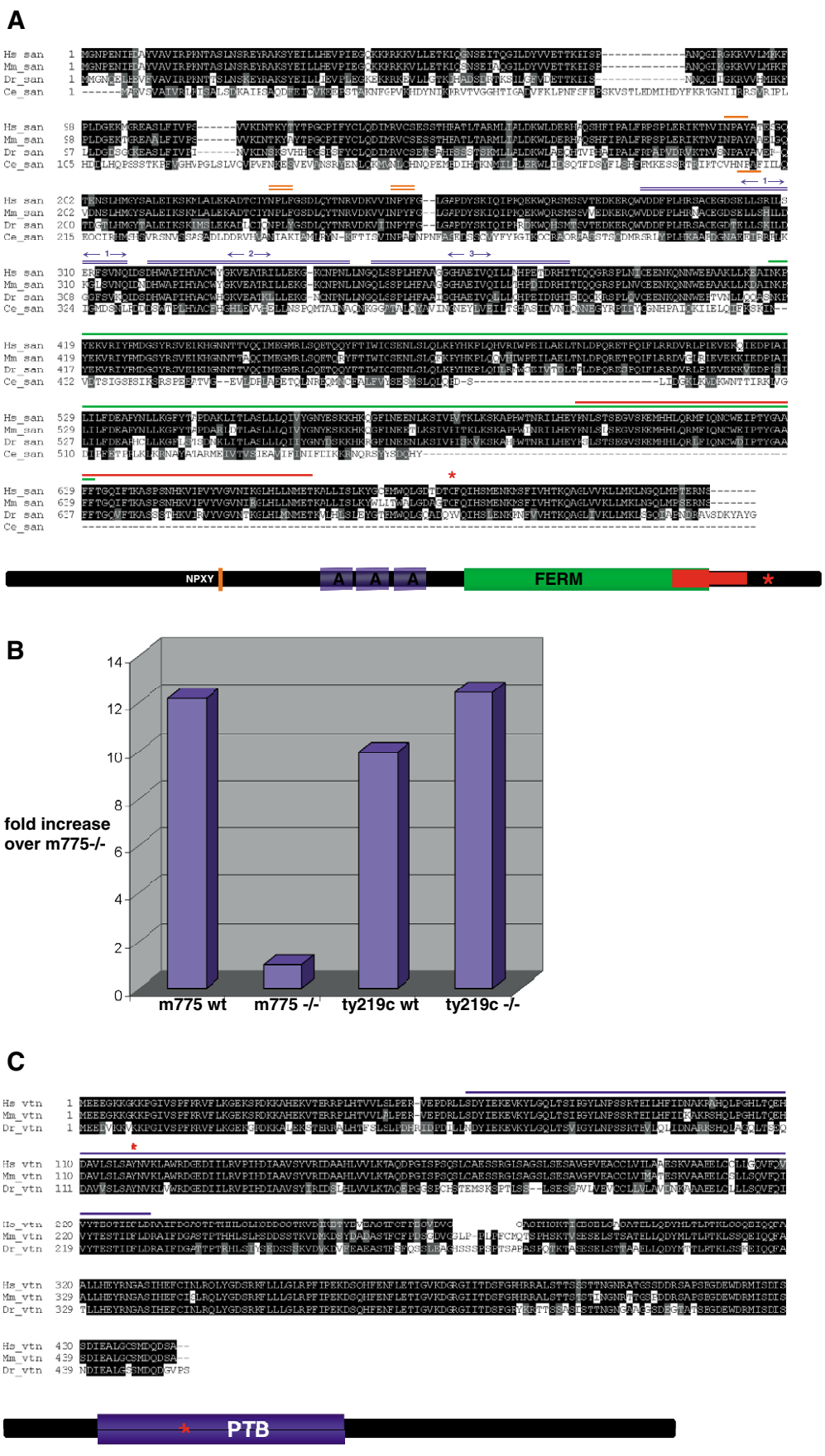

Fig. 2. The *san* and *vtn* loci encode the zebrafish homologs of CCM1 and CCM2. (**A**) The zebrafish (Dr) San (CCM1) protein sequence is aligned with the *C. elegans* (Ce), mouse (Mm) and human (Hs) homologs, demonstrating strong identity among the three vertebrate genes. The *N*-terminal NPxY motif indicated by the single brown line (NPAY, residues 191-194 of the zebrafish protein and residues 192-195 of the mouse and human protein) is altered in the *C. elegans* homolog to NPAF. This motif is associated with interaction of *san* with both ICAP1 and *vtn* (Zawistowski et al., 2002; Zawistowski et al., 2005; Zhang et al., 2001). The other two NPxF/Y motifs, indicated by brown double lines, were not required for interaction of *san* with *vtn* (Zawistowski et al., 2005). The three blue double lines indicate the location of the ankyrin repeats and the single green line denotes the FERM domain. The red asterisk indicates the position of the Y→stop mutation in the zebrafish *san* ty219c allele. The protein motifs are shown schematically below the sequence. The red asterisk again denotes the *san* ty219c mutation and the region of the protein shown in red corresponds to exon 14, deleted in the *san* m775 allele. (**B**) Real-time PCR analysis was used to examine the level of *san* mRNA message containing exon 14. mRNA isolated from m775 wild-type siblings, and both wild-type and mutant ty219c embryos show levels of exon 14-containing message 10-fold greater than in the *san* m775 mutant embryos (m775 –/– level set to 1 for comparison). (**C**) The Vtn (CCM2) protein is very well conserved among vertebrates [the zebrafish (Dr) Vtn protein sequence is aligned with the mouse (Mm) and human (Hs) homologs, no *C. elegans* homolog is detectable]. The single blue line indicates the sequence corresponding to the PTB domain and the red asterisk indicates the position of the Y→stop mutation in the zebrafish *vtn* m201 allele. The Vtn protein shown schematically below the sequence illustrates the position of the PTB domain and site of the *vtn* m201 mutation.

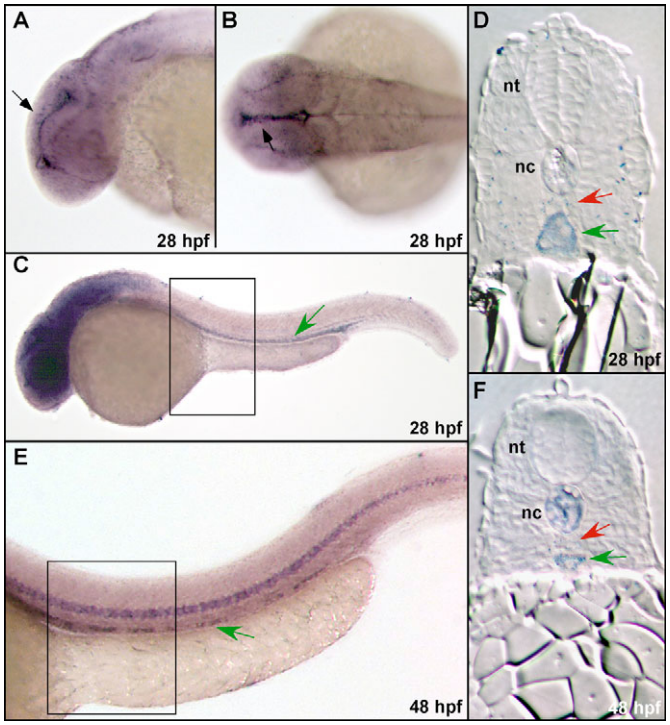

Fig. 3. In-situ analysis of *san* mRNA expression. The *san* mRNA is expressed in the ventricular zone (black arrow) and diffusely throughout the brain at 28 hpf (**A**,**B**). Expression is also detectable at this stage in the posterior cardinal vein (green arrow) as illustrated by whole-mount (**C**) and in section (**D**). At 48 hpf, *san* expression is detectable in the notochord with patchy expression in the vein (**E**). The staining in the vein is clearly visible from sections through the trunk (**F**). The position of the dorsal aorta is indicated by the red arrow. The boxed region in C and E represent the region shown in the sections. nc, notochord; nt, neural tube.

vtn

The complete vtn gene is comprised of 10 coding exons with a deduced amino acid sequence of 455 amino acids. The predicted protein is cytosolic with a molecular weight of 50 kDa. The protein has one recognizable protein motif, a PTB domain (amino acids 61-229). The *vtn* protein is highly conserved across vertebrates and encodes the zebrafish homolog of the human gene associated with CCM2 (MGC4607, malcalverin; Fig. 2C). The m201 allele of *vtn* (Stainier et al., 1996) is defined by a C to A transversion within codon 119 of exon 4 (TAC→TAA). This would cause a tyrosine change to a stop codon (Y→stop, Fig. 2C). This results in the formation of a truncated protein with an incomplete PTB domain.

Morpholino confirmation and RNA rescue of genetic lesions

san

We employed an antisense morpholino designed to block splicing at the donor site at the end of exon 14 of the *san* mRNA (data not shown) (Draper et al., 2001; Ekker, 2000; Mably et al., 2003). Injection of this morpholino at the 1-cell stage resulted in a complete copy of the mutant phenotype (>95% of embryos show the phenotype, n>1000). Analysis by RT-PCR using primers within exons flanking exon 14 revealed a partial in-frame loss of exon 14 sequence, confirming that loss of part of the FERM domain is sufficient to reproduce the mutant phenotype (data not shown). Mock-injected controls reveal no effect on the *san* PCR products.

We also designed a morpholino to block splicing of the donor site at the end of exon 1 in an attempt to create a truncated protein (through the excision of 5′ exon sequence and disruption of the reading frame). However, this morpholino caused deletion of 75 base pairs (bp), predicting in-frame loss of 25 amino acids, due to the recruitment of a splice donor site within exon 1 (data not shown). Interestingly, loss of these 25 amino acids was sufficient to produce a complete phenocopy, implicating the *N*-terminus of the protein as essential for normal function. Injection of mRNA derived from the predicted full-length *san* cDNA was unable to rescue the mutant phenotype. At high levels, expression of *san* mRNA in wild-type embryos impaired early development, probably due to misexpression of San in all cells.

vtn

A morpholino was designed to the donor site at the end of exon 2 of the *vtn* gene. Injection of this morpholino at the 1-cell stage results in a complete phenocopy of the *vtn* mutation (>95% phenocopy with n>1000, data not shown). Analysis by RT-PCR using primers within exons flanking exon 2 and sequence analysis of the products revealed transcripts predicting both a partial and complete loss of exon 2 sequence (data not shown). Injection of predicted *vtn* mRNA into progeny of *vtn* heterozygote matings rescued embryos completely (Table 2).

san and *vtn* mRNA expression

Analysis of *san* mRNA by whole-mount in-situ hybridization at 28 hpf revealed staining in the ventricular zone of the brain (Fig. 3A,B), with weaker staining throughout the entire brain, and in the posterior cardinal vein (Fig. 3C,D). The venous expression was maintained at 48 hpf, although expression was patchy (Fig. 3E,F). At 48 hpf there was also prominent notochord staining.

Similarly, strong expression of *vtn* mRNA at 28 hpf was detected in the brain ventricular zone (Fig. 4A-D) with weaker expression in the vein (Fig. 4E,G). *vtn* mRNA was also obvious in the posterior intermediate cell mass at this stage (Fig. 4A,E,F). By 48 hpf,

Table 2. Rescue of *vtn* mutant phenotype by mRNA injection.

	Wild type	Intermediate	Mutant
100 ng/μl wild-type *vtn* RNA in m201 × m201	455 (92.8%)	40 (8.0%)	1 (0.2%)
100 ng/μl wild-type *san* RNA in m201 × m201	37 (75.5%)	0 (0%)	12 (24.5%)
Mock injected in m201 × m201	142 (74%)	0 (0%)	50 (26%)
100 ng/μl wild-type *vtn* RNA in m775 × m775	69 (74%)	0 (0%)	24 (26%)
100 ng/μl wild-type *san* RNA in m775 × m775	183 (75%)	0 (0%)	61 (25%)
Mock injected in m775 × m775	60 (74%)	0 (0%)	19 (26%)

Injection of *vtn* mRNA, but not *san* mRNA, into the progeny of m201 heterozygotes is able to rescue the *vtn* mutant phenotype. Neither *san* nor *vtn* mRNA injection is able to rescue the *san* mutant phenotype.

expression of *vtn* was weaker, but was detectable in the vein (Fig. 4H-J). At both 28 and 48 hpf, a low level of *vtn* mRNA was detectable in a region near the dorsal aorta (Fig. 4G,J).

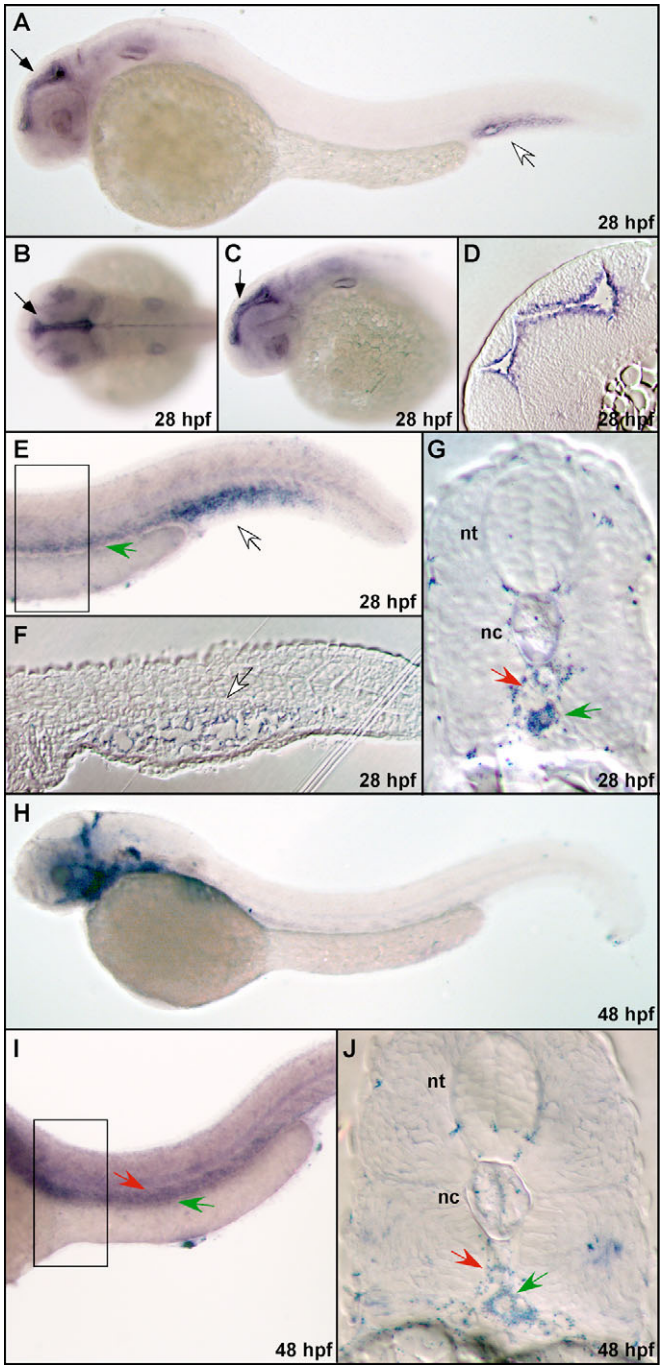

Fig. 4. In-situ analysis of *vtn* mRNA expression. The *vtn* mRNA is robustly expressed in the ventricular zone (black arrow) at 28 hpf (**A-C**), also shown in section in **D**. Expression is also strong in the intermediate cell mass (A,**E,F**, white arrow). Lengthened staining also reveals *vtn* message in the vein (E, green arrow) confirmed by sectioning (**G**). At 48 hpf, *vtn* is expressed in the brain and diffusely in the branchial arches (**H**). Expression in the vein is detectable by whole-mount (**I**) and from sections (**J**), but is weaker than expression of *san* at this stage. The position of the dorsal aorta is indicated by the red arrow. The boxed region in E and I represent the region shown in the sections. nt, neural tube; nc, notochord.

Co-morpholino evidence of interaction of *san*, *vtn* and *heg*

The similarity of phenotype between *san*, *vtn* and *heg*, along with the predicted interactive ability of protein motifs (PTB domain of *vtn* and NPxY motif of *san*/NPxF motif of *heg*) suggested that these proteins might be part of a pathway that controls concentric growth of the heart. To examine this, we lowered amounts of each protein by morpholino injection to a level at which fewer than 10% of embryos demonstrated a complete phenocopy. Combinations of morpholinos were then injected at these doses to determine if the effects of these morpholinos are additive. Injection of *san* and *vtn* together at these doses resulted in a dramatic increase in the percentage of embryos exhibiting complete phenocopy (Fig. 5; see Table S1 in the supplementary material). When injected together with either the *san* or *vtn* morpholino at low doses, the *heg* combinations also produce a significant increase in phenocopy level (Fig. 5). These results suggest that *san*, *vtn* and *heg* interact.

DISCUSSION

The thickening of the myocardium is essential to generate the higher blood pressures characteristic of vertebrate physiology. The primitive heart tube forms before physiological function, suggesting that the primary determinant of the tube's initial dimensions are not dictated by physiological forces. In fact, there is evidence that the size of the heart correlates with overall body growth (termed allometry) (Gould, 1966). After transplantation of precardiac mesoderm between two amphibian species, tissue from the faster growing *Amblystoma tigrinum* transferred to *Amblystoma punctatum* results in hearts that grow more rapidly than in the native host (Copenhaver, 1939). Flow and pressure clearly modify subsequent patterns of growth in the embryonic ventricle, as

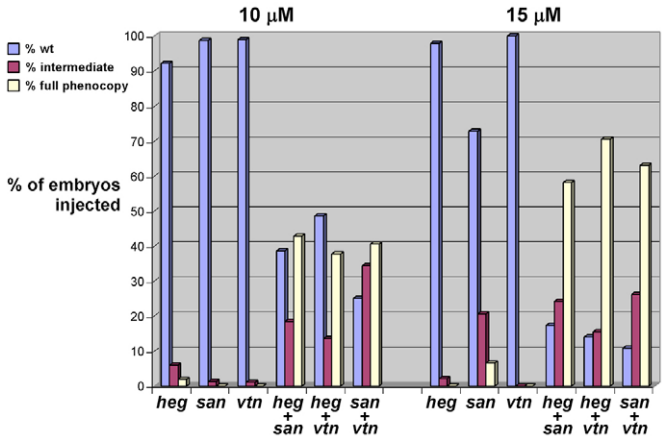

Fig. 5. Morpholino co-injections reveal evidence of interactions between *san*, *vtn* and *heg*. Injection of low doses (10 and 15 μmol/l) of each morpholino alone is unable to produce large number of embryos with the characteristic enlarged heart and thin-walled myocardium. However, by injection of combinations of any two of the *san*, *vtn* and *heg* morpholinos, a dramatic increase in the level of phenocopy is observed (indicated by the increase in the yellow bars) with a concomitant decrease in the level of wild-type embryos (blue bars). A number of embryos (indicated by the red bars) display a phenotype intermediate between wild type and mutant, characterized by a less dramatic dilation of the heart and some with weak circulation. *heg*, heg exon 11 donor morpholino injected; *san*, *san* exon 1 donor morpholino injected; *vtn*, *vtn* exon 2 morpholino injected.

illustrated by the formation of congenital defects in chick embryos following constriction of the outflow tract during development of the heart tube (Gessner, 1966).

Through the characterization of two zebrafish mutants, *san* and *vtn*, we introduce here a new genetic pathway, one essential for myocardial growth and thickening of the ventricular wall in vertebrates. In the hearts of these mutants, both atrial and ventricular chambers are correctly specified and hearts possess myofibrils and are able to contract. Although the number of cells in the heart muscle wall is normal, there is no concentric growth. Rather, the cells proliferate along the circumference of the heart, leading to the formation of a hugely dilated heart consisting of a single layer of myocardium. The targeted deletion of the homolog of *san* in mice also results in an enlargement of the cardiac chambers, particularly the atrium (Whitehead et al., 2004). However, the hearts loop normally and develop endocardial cushions (Whitehead et al., 2004). The absence of looping and the loss of endocardial cushion formation in the zebrafish mutant may represent secondary affects on the morphology of the heart resulting from the severe cardiac dilation observed or possible variations in timing requirements between species for these genes during development.

CCM1 (San) interacts with integrin cytoplasmic domain associated protein-1 (ICAP-1), a modulator of integrin signaling (Zawistowski et al., 2002; Zhang et al., 2001). Like Vtn (CCM2), this protein contains a PTB domain. This PTB domain is essential for the interaction of ICAP-1 with the NPxY motif within the cytoplasmic tail of β1 integrin (Chang et al., 1997; Zhang and Hemler, 1999) and with the NPxY domain of CCM1 (amino acids NPAY, see Fig. 2A). These interactions with CCM1 and/or β1 integrin have been proposed to modulate cell-cell and cell-extracellular matrix communication, essential for a variety of processes, including cell migration and maintenance of cellular morphology.

Consistent with the morpholino data indicating that *san*, *vtn* and *heg* interact to control myocardial thickening in the zebrafish heart during development, recent work has demonstrated a physical interaction between CCM1 (San) and CCM2 (Vtn) by immunoprecipitation and FRET analysis (Zawistowski et al., 2005). Unlike the interaction between ICAP1 and CCM1, binding to CCM2 was not completely eliminated by mutagenesis of the *N*-terminal NPAY motif in CCM1, although this motif was shown to be involved in CCM2-binding (Zawistowski et al., 2005). These results suggest that CCM2 can bind to additional motifs in CCM1. However, mutagenesis of the other two NPxF/Y motifs in CCM1 (indicated in Fig. 2A) revealed that they were not strong sites of CCM2 interaction (Zawistowski et al., 2005). In addition, the murine CCM2 homolog (OSM, for osmosensing scaffold for MEKK3) serves as a scaffold protein for MEKK3-mediated p38 MAPK phosphorylation during osmotic shock, interacting directly with Rac1, MEKK3 and MKK3 (Uhlik et al., 2003). This complex also includes CCM1 (San), as demonstrated by co-immunoprecipitation (Zawistowski et al., 2005).

The results of our co-morpholino experiments also implicate Heg as another member of this complex interactome. The *heg* gene has been shown to be an endocardial signal required for the concentric thickening of the myocardium. Loss of function of this gene in zebrafish generates a phenotype indistinguishable from *san* and *vtn* (Mably et al., 2003). We have demonstrated that knockdown of combinations of the three zebrafish genes show synergistic effects, strengthening the contention that the genes disrupted in human CCM function through a common molecular pathway.

The phenotype of the *san* and *vtn* mutant embryonic heart, like *heg*, most closely resembles that of the heart in *cloche* (*clo*) mutant zebrafish, which lack endocardium and other endothelium (Liao et al., 1997; Parker and Stainier, 1999; Stainier et al., 1996). Based on the expression pattern of the *san* and *vtn* genes, it is difficult to conclude which of the two cell types in the hearts is primarily affected, although the expression of *san* and *vtn* in the vasculature and *heg* in the endocardium (Mably et al., 2003), together with the similarity to the *clo* phenotype, suggest a role for endocardial cells in growth of the adjacent myocardium. The dilated cardiac chambers of the *san* and *vtn* mutants exhibit a severe thinning and dilation that is also reminiscent of the dilated capillary walls observed in PDGF-B-deficient mice, which exhibit impaired recruitment of pericytes because of the loss of PDGF-B signaling (Lindahl et al., 1997). It is postulated that one of the roles of the pericytes is to contribute to the mechanical stability of the capillary wall, and in their absence microaneurysms develop. Analogous to these lesions, the enlarged cardiac chambers of the *san* and *vtn* mutants reflects an inability of the endocardial cell layer to instruct the adjacent layer of myocardial muscle to thicken.

During the initial stages of embryonic development, the endocardium may help maintain the structural integrity of the heart by serving as a framework for the surrounding myocardium. Furthermore, although the number of endocardial cells in the two mutants is similar to wild type, a small population of cells may be recruited to the endocardium from other sites, such as the intermediate cell mass (ICM), where *vtn* is expressed, and these cells may migrate through the vasculature to contribute to the maturation of the endocardium. Indeed, the endocardium has been proposed to be the site of hematopoiesis before onset of definitive hematopoiesis in the kidney at 4-5 dpf seeded by cells from the blood islands within the ICM (Al-Adhami and Kunz, 1977). The expression of both *san* and *vtn* in the vein may represent this migrating population of cells that are essential to maturation of the endocardium and, indirectly, the adjacent myocardium through the supply of growth signals.

The human homologs of the zebrafish *san* (CCM1) and *vtn* (CCM2) genes are disrupted in cerebral cavernous malformations, a disorder characterized by the formation of enlarged and thin-walled vascular malformations in the CNS (Gil-Nagel et al., 1995; Zabramski et al., 1999). The mechanism by which disruptions in these genes produce these characteristic venous lesions is undefined. However, a similar process to that proposed to explain the zebrafish defects might lay at the basis of these vascular anomalies as well as the defect in the mouse CCM1 (*san*) knockout, which reveals an essential role for this gene in vascular development (Whitehead et al., 2004).

This work reveals the molecular basis for a mechanism of cardiac growth distinct from those that control cell proliferation. This process determines the direction of growth and is essential for the thickening of the ventricular wall. Formation of the myocardium is contingent on the presence of an intact endocardium and requires reciprocal signaling between the two cell types, facilitated through a genetic module consisting of *san*, *vtn* and *heg*.

We thank C. Simpson for histological sectioning, and B. Roman, N. Lawson and B. Weinstein for the transgenic *(fli1:nEGFP)*^{y7} zebrafish. We thank Joanne Chan for critical review of this manuscript. This work was supported by grants from NIH [5R01HL49579,5R01DK55383 (MCF) and 5R01HL63206-04 (JDM/MCF)], and by a sponsored research agreement with Genentech.

Supplementary material

Supplementary material for this article is available at
http://dev.biologists.org/cgi/content/full/133/16/3139/DC1

References

Al-Adhami, M. A. and Kunz, Y. W. (1977). Ontogenesis of haematopoietic sites in brachydanio rerio (hamilton-buchanan) (teleostei). *Dev. Growth Differ.* **19**, 171-179.

Bretscher, A., Edwards, K. and Fehon, R. G. (2002). ERM proteins and merlin: integrators at the cell cortex. *Nat. Rev. Mol. Cell Biol.* **3**, 586-599.

Burge, C. B. and Karlin, S. (1998). Finding the genes in genomic DNA. *Curr. Opin. Struct. Biol.* **8**, 346-354.

Calderwood, D. A., Fujioka, Y., de Pereda, J. M., Garcia-Alvarez, B., Nakamoto, T., Margolis, B., McGlade, C. J., Liddington, R. C. and Ginsberg, M. H. (2003). Integrin beta cytoplasmic domain interactions with phosphotyrosine-binding domains: a structural prototype for diversity in integrin signaling. *Proc. Natl. Acad. Sci. USA* **100**, 2272-2277.

Chang, D. D., Wong, C., Smith, H. and Liu, J. (1997). ICAP-1, a novel beta1 integrin cytoplasmic domain-associated protein, binds to a conserved and functionally important NPXY sequence motif of beta1 integrin. *J. Cell Biol.* **138**, 1149-1157.

Chen, J. N., Haffter, P., Odenthal, J., Vogelsang, E., Brand, M., van Eeden, F. J., Furutani-Seiki, M., Granato, M., Hammerschmidt, M., Heisenberg, C. P. et al. (1996). Mutations affecting the cardiovascular system and other internal organs in zebrafish. *Development* **123**, 293-302.

Copenhaver, W. (1939). Some observations on the growth and function of heteroplastic heart grafts. *J. Exp. Zool.* **82**, 239-271.

Denier, C., Goutagny, S., Labauge, P., Krivosic, V., Arnoult, M., Cousin, A., Benabid, A. L., Comoy, J., Frerebeau, P., Gilbert, B. et al. (2004). Mutations within the MGC4607 gene cause cerebral cavernous malformations. *Am. J. Hum. Genet.* **74**, 326-337.

Draper, B. W., Morcos, P. A. and Kimmel, C. B. (2001). Inhibition of zebrafish fgf8 pre-mRNA splicing with morpholino oligos: a quantifiable method for gene knockdown. *Genesis* **30**, 154-156.

Driever, W., Solnica-Krezel, L., Schier, A. F., Neuhauss, S. C., Malicki, J., Stemple, D. L., Stainier, D. Y., Zwartkruis, F., Abdelilah, S., Rangini, Z. et al. (1996). A genetic screen for mutations affecting embryogenesis in zebrafish. *Development* **123**, 37-46.

Ekker, S. C. (2000). Morphants: a new systematic vertebrate functional genomics approach. *Yeast* **17**, 302-306.

Ewing, B. and Green, P. (1998). Base-calling of automated sequencer traces using phred. II. Error probabilities. *Genome Res.* **8**, 186-194.

Ewing, B., Hillier, L., Wendl, M. C. and Green, P. (1998). Base-calling of automated sequencer traces using phred. I. Accuracy assessment. *Genome Res.* **8**, 175-185.

Gessner, I. H. (1966). Spectrum of congenital cardiac anomalies produced in chick embryos by mechanical interference with cardiogenesis. *Circ. Res.* **18**, 625-633.

Gil-Nagel, A., Wilcox, K. J., Stewart, J. M., Anderson, V. E., Leppik, I. E. and Rich, S. S. (1995). Familial cerebral cavernous angioma: clinical analysis of a family and phenotypic classification. *Epilepsy Res.* **21**, 27-36.

Gordon, D., Abajian, C. and Green, P. (1998). Consed: a graphical tool for sequence finishing. *Genome Res.* **8**, 195-202.

Gould, S. J. (1966). Allometry and size in ontogeny and phylogeny. *Biol. Rev. Camb. Philos. Soc.* **41**, 587-640.

Hu, N., Sedmera, D., Yost, H. J. and Clark, E. B. (2000). Structure and function of the developing zebrafish heart. *Anat. Rec.* **260**, 148-157.

Jowett, T. and Lettice, L. (1994). Whole-mount in situ hybridizations on zebrafish embryos using a mixture of digoxigenin- and fluorescein-labelled probes. *Trends Genet.* **10**, 73-74.

Knapik, E. W., Goodman, A., Atkinson, O. S., Roberts, C. T., Shiozawa, M., Sim, C. U., Weksler-Zangen, S., Trolliet, M. R., Futrell, C., Innes, B. A. et al. (1996). A reference cross DNA panel for zebrafish (Danio rerio) anchored with simple sequence length polymorphisms. *Development* **123**, 451-460.

Laberge-le Couteulx, S., Jung, H. H., Labauge, P., Houtteville, J. P., Lescoat, C., Cecillon, M., Marechal, E., Joutel, A., Bach, J. F. and Tournier-Lasserve, E. (1999). Truncating mutations in CCM1, encoding KRIT1, cause hereditary cavernous angiomas. *Nat. Genet.* **23**, 189-193.

Liao, W., Bisgrove, B. W., Sawyer, H., Hug, B., Bell, B., Peters, K., Grunwald, D. J. and Stainier, D. Y. (1997). The zebrafish gene cloche acts upstream of a flk-1 homologue to regulate endothelial cell differentiation. *Development* **124**, 381-389.

Lindahl, P., Johansson, B. R., Leveen, P. and Betsholtz, C. (1997). Pericyte loss and microaneurysm formation in PDGF-B-deficient mice. *Science* **277**, 242-245.

Mably, J. D., Mohideen, M.-A. P. K. Burns, C. G., Chen, J.-N. and Fishman, M. C. (2003). *heart of glass* regulates the concentric growth of the heart in zebrafish. *Curr. Biol.* **13**, 2138-2147.

Michelmore, R. W., Paran, I. and Kesseli, R. V. (1991). Identification of markers linked to disease-resistance genes by bulked segregant analysis: a rapid method to detect markers in specific genomic regions by using segregating populations. *Proc. Natl. Acad. Sci. USA* **88**, 9828-9832.

Milan, D. J., Giokas, A. C., Serluca, F. C., Peterson, R. T. and Macrae, C. A. (2006). Notch1b and neuregulin are required for specification of central cardiac conduction tissue. *Development* **133**, 1125-1132.

Mosavi, L. K., Cammett, T. J., Desrosiers, D. C. and Peng, Z. Y. (2004). The ankyrin repeat as molecular architecture for protein recognition. *Protein Sci.* **13**, 1435-1448.

Parker, L. and Stainier, D. Y. (1999). Cell-autonomous and non-autonomous requirements for the zebrafish gene cloche in hematopoiesis. *Development* **126**, 2643-2651.

Roman, B. L., Pham, V. N., Lawson, N. D., Kulik, M., Childs, S., Lekven, A. C., Garrity, D. M., Moon, R. T., Fishman, M. C., Lechleider, R. J. et al. (2002). Disruption of acvrl1 increases endothelial cell number in zebrafish cranial vessels. *Development* **129**, 3009-3019.

Rottbauer, W., Baker, K., Wo, Z. G., Mohideen, M. A., Cantiello, H. F. and Fishman, M. C. (2001). Growth and function of the embryonic heart depend upon the cardiac-specific L-type calcium channel alpha1 subunit. *Dev. Cell* **1**, 265-275.

Rottbauer, W., Saurin, A. J., Lickert, H., Shen, X., Burns, C. G., Wo, Z. G., Kemler, R., Kingston, R., Wu, C. and Fishman, M. (2002). Reptin and pontin antagonistically regulate heart growth in zebrafish embryos. *Cell* **111**, 661-672.

Sahoo, T., Johnson, E. W., Thomas, J. W., Kuehl, P. M., Jones, T. L., Dokken, C. G., Touchman, J. W., Gallione, C. J., Lee-Lin, S. Q., Kosofsky, B. et al. (1999). Mutations in the gene encoding KRIT1, a Krev-1/rap1a binding protein, cause cerebral cavernous malformations (CCM1). *Hum. Mol. Genet.* **8**, 2325-2333.

Shu, X., Cheng, K., Patel, N., Chen, F., Joseph, E., Tsai, H. J. and Chen, J. N. (2003). Na,K-ATPase is essential for embryonic heart development in the zebrafish. *Development* **130**, 6165-6173.

Stainier, D. Y. and Fishman, M. C. (1992). Patterning the zebrafish heart tube: acquisition of anteroposterior polarity. *Dev. Biol.* **153**, 91-101.

Stainier, D. Y., Fouquet, B., Chen, J. N., Warren, K. S., Weinstein, B. M., Meiler, S. E., Mohideen, M. A., Neuhauss, S. C., Solnica-Krezel, L., Schier, A. F. et al. (1996). Mutations affecting the formation and function of the cardiovascular system in the zebrafish embryo. *Development* **123**, 285-292.

Turner, D. L. and Weintraub, H. (1994). Expression of achaete-scute homolog 3 in Xenopus embryos converts ectodermal cells to a neural fate. *Genes Dev.* **8**, 1434-1447.

Uhlik, M. T., Abell, A. N., Johnson, N. L., Sun, W., Cuevas, B. D., Lobel-Rice, K. E., Horne, E. A., Dell'Acqua, M. L. and Johnson, G. L. (2003). Rac-MEKK3-MKK3 scaffolding for p38 MAPK activation during hyperosmotic shock. *Nat. Cell Biol.* **5**, 1104-1110.

Whitehead, K. J., Plummer, N. W., Adams, J. A., Marchuk, D. A. and Li, D. Y. (2004). Ccm1 is required for arterial morphogenesis: implications for the etiology of human cavernous malformations. *Development* **131**, 1437-1448.

Yelon, D., Horne, S. A. and Stainier, D. Y. (1999). Restricted expression of cardiac myosin genes reveals regulated aspects of heart tube assembly in zebrafish. *Dev. Biol.* **214**, 23-37.

Zabramski, J. M., Henn, J. S. and Coons, S. (1999). Pathology of cerebral vascular malformations. *Neurosurg. Clin. N. Am.* **10**, 395-410.

Zawistowski, J. S., Serebriiskii, I. G., Lee, M. F., Golemis, E. A. and Marchuk, D. A. (2002). KRIT1 association with the integrin-binding protein ICAP-1: a new direction in the elucidation of cerebral cavernous malformations (CCM1) pathogenesis. *Hum. Mol. Genet.* **11**, 389-396.

Zawistowski, J. S., Stalheim, L., Uhlik, M. T., Abell, A. N., Ancrile, B. B., Johnson, G. L. and Marchuk, D. A. (2005). CCM1 and CCM2 protein interactions in cell signaling: implications for cerebral cavernous malformations pathogenesis. *Hum Mol Genet*. **14**, 2521-2531.

Zhang, J., Clatterbuck, R. E., Rigamonti, D., Chang, D. D. and Dietz, H. C. (2001). Interaction between krit1 and icap1alpha infers perturbation of integrin beta1-mediated angiogenesis in the pathogenesis of cerebral cavernous malformation. *Hum. Mol. Genet.* **10**, 2953-2960.

Zhang, X. A. and Hemler, M. E. (1999). Interaction of the integrin beta1 cytoplasmic domain with ICAP-1 protein. *J. Biol. Chem.* **274**, 11-19.

Table S1. Morpholino co-injections reveal evidence of interactions between *san*, *vtn* and *heg*

	Wild type	Intermediate	Mutant
10 μM *heg*_e11i11	94 (92.2%)	6 (5.9%)	2 (1.9%)
10 μM *san*_e1i1	86 (98.9%)	1 (1.1%)	0 (0%)
10 μM *vtn*_e1i1	90 (98.9%)	1 (1.1%)	0 (0%)
10 μM *heg*_e11i11 + 10 μM *san*_e1i1	46 (38.6%)	22 (18.5%)	51 (42.9%)
10 μM *heg*_e11i11 + 10 μM *vtn*_e1i1	18 (48.7%)	5 (13.5%)	14 (37.8%)
10 μM *san*_e1i1 + 10 μM *vtn*_e1i1	8 (25.0%)	11 (34.4%)	13 (40.6%)
15 μM *heg*_e11i11	97 (98.0%)	2 (2.0%)	0 (0%)
15 μM *san*_e1i1	110 (72.9%)	31 (20.5%)	10 (6.6%)
15 μM *vtn*_e1i1	121 (100%)	0 (0%)	0 (0%)
15 μM *heg*_e11i11 + 15 μM *san*_e1i1	18 (17.5%)	25 (24.3%)	60 (58.2%)
15 μM *heg*_e11i11 + 15 μM *vtn*_e1i1	18 (14.0%)	20 (15.5%)	91 (70.5%)
15 μM *san*_e1i1 + 15 μM *vtn*_e1i1	9 (10.7%)	22 (26.2%)	53 (63.1%)

Injection of *heg*, *san* or *vtn* morpholinos alone at 10 μM or 15 μM is unable to produce a complete phenocopy. However, injection of combinations of any two of these morpholinos produces a dramatic increase in the level of phenocopy. A number of embryos display a phenotype intermediate between wild type and mutant, characterized by a less dramatic dilation of the heart and some with weak circulation. These results are displayed graphically in Fig. 5.